JOURNAL OF MATERIALS SCIENCE 27 (1992) 6481–6489

High temperature creep behaviour of an Ni–Cr–W–B alloy

H. M. TAWANCY
Materials Characterization Laboratory, Metrology, Standards and Materials Division, Research Institute, King Fahd University of Petroleum and Minerals, P.O. Box 1639, Dhahran 31261, Saudi Arabia

The high-temperature creep behaviour of a solid-solution strengthened Ni–Cr–W–B alloy was studied, with emphasis on microstructural parameters. Creep strength was determined from tests conducted at 925 °C/40 MPa. Various techniques of analytical electron microscopy were used to characterize the microstructure and microchemical composition. A number of microstructural parameters which promote creep strength, including (1) pinning of grain boundaries by tungsten-rich M_6C carbide, (2) relatively low stacking-fault energy, and (3) boron segregation to $M_{23}C_6$ carbide, were identified. However, their beneficial effects were suppressed by the initial presence of discontinuously precipitated $M_{23}C_6$ carbide at grain boundaries which accelerated intergranular cracking. Suppression of the discontinuous grain-boundary reaction and a significant improvement in creep strength could be achieved by a proper heat treatment which appeared to induce a sufficiently high defect density promoting intragranular carbide precipitation. Competition between intergranular and intragranular precipitation was found to be influenced by an external stress. Strengthening by intragranular carbide precipitates appeared to occur by an attractive interaction with dislocations. Dislocations bowing out at subboundaries, cross-slip, motion of jogged screw dislocations and generation of dislocations at high-angle grain boundaries appeared to operate simultaneously as strain-producing mechanisms during steady-state creep.

1. Introduction

One of the newly developed wrought high-temperature alloys is the Ni–Cr–W–B Haynes* alloy no. 230 [1, 2]. Table I lists its nominal chemical composition. Alloy 230 is characterized by a potentially useful combination of high-temperature mechanical strength, environmental resistance and thermal stability [1, 2]. Essentially, the alloy derives its strength from solid solution. However, the high-temperature creep strength can be promoted by precipitation of $M_{23}C_6$ carbide. Owing to the characteristic properties of the alloy, it can find a wide variety of component applications in the aerospace and chemical process industries.

Among the important parameters in designing alloys for high-temperature applications is the low-strain creep strength and creep–rupture life [3, 4]. It is well known that the creep strength is a sensitive function of microstructure. For a given alloy, the microstructural parameters which can significantly influence its creep strength include: grain size, stacking fault energy, subgrain size, subboundary misorientation, and distribution of dislocations at subboundaries and in the interiors of the subgrains [5].

It was the objective of this investigation to study the high-temperature creep behaviour of alloy 230 with particular emphasis on: (1) the effect of initial microstructure, (2) the microstructural changes which occur during creep deformation, and (3) the role of boron.

2. Experimental procedure

An alloy sheet (~ 1.3 mm thick) of commercial grade was used in this study. Specimens were solution annealed at 1230 °C for 15 min as recommended by the

TABLE I Nominal chemical composition of alloy 230

(wt %)	
Ni	Balance
Cr	22
W	14
Mo	2
Co	5[a]
Fe	3[a]
Mn	0.5
Si	0.4
Al	0.3
C	0.1
La	0.02
B	0.005

[a] Maximum.

---

* Haynes is a registered trademark of Hayens International Company.

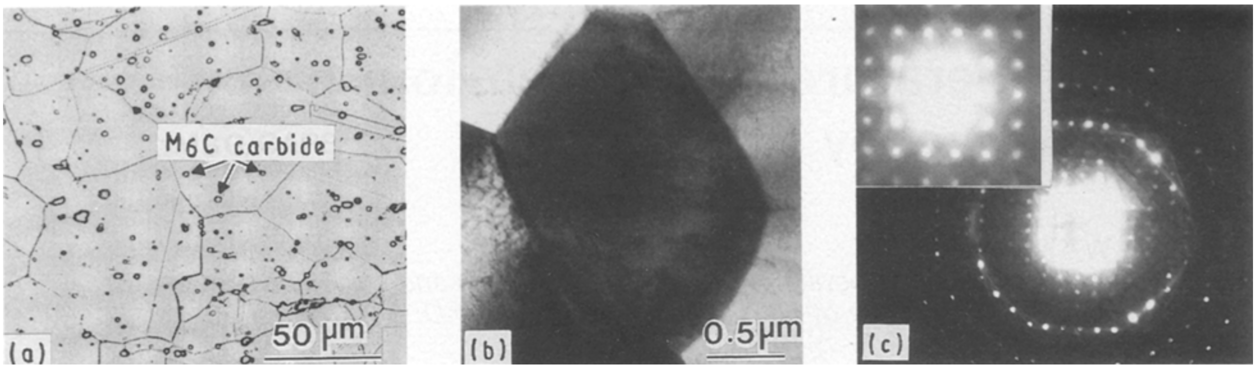

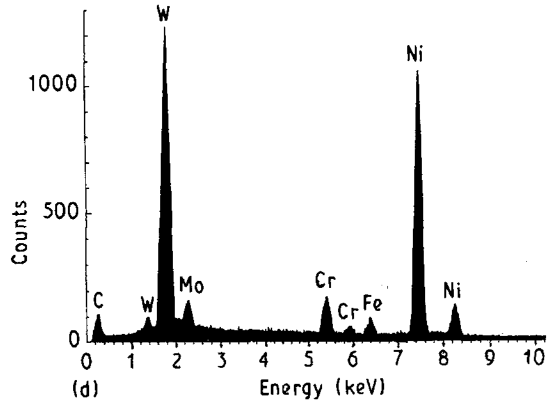

Figure 1 Identification of a tungsten-rich M_6C carbide in the annealed condition. (a) Light optical micrograph illustrating a typical grain structure. (b) Bright-field STEM image illustrating an M_6C carbide particle at a triple point. (c) [0 0 1] convergent beam diffraction pattern derived from the particle in (b); the zero-order Laue zone is shown in the inset. (d) X-ray spectrum derived from the particle in (b).

manufacturer. To determine the effect of cooling rate from the solution annealing temperature on initial microstructure and creep strength, some specimens were air-cooled and others were water-quenched. Creep tests were conducted in air at 925 °C/40 MPa (50.8 mm gauge length).

Specimens for light optical metallography were etched in a solution consisting of 80% concentrated hydrochloric acid and 20% chromic acid (15 mol % concentration). Fine microstructural details were characterized using an analytical electron microscope equipped with an ultra-thin window X-ray detector and an electron energy loss spectrometer. Thin-foil specimens were prepared by the jet polishing technique in a solution consisting of 30% nitric acid in methanol at about − 20 °C. All specimens were examined at an accelarating voltage of 200 kV. A scanning electron microscope was used to characterize the creep fracture mode.

3. Results and discussion

3.1. Initial microstructure

Fig. 1 summarizes typical microstructural features in the annealed condition. Secondary phase particles were observed to be randomly dispersed throughout the grain structure as illustrated in the light optical micrograph of Fig. 1a. By means of convergent beam diffraction (CBD) and energy dispersive X-ray spectroscopy (EDXS), those particles were identified to be of an M_6C carbide of the type Ni_3W_3C (face-centred cubic; $a = 1.11$ nm) as illustrated in Fig. 1b–d.

Random dispersion of M_6C carbide particles as observed in Fig. 1a could result from their precipitation during thermomechanical processing. Owing to the relatively high stability of tungsten-rich M_6C carbide, it would be expected to resist effectively grain-boundary migration at elevated temperatures, particularly when present at triple points, as shown in Fig. 1b. Because grain-boundary migration accompanies grain-boundary sliding [6–8], the presence of tungsten-rich M_6C carbide particles at grain boundaries could reduce the sliding rate.

On the finer scale of transmission electron microscopy, the grain-boundary structure was found to be sensitive to cooling rate from the annealing temperature. For both air-cooled and water-quenched specimens, the grain boundaries were observed to contain precipitates identified to be of the chromium-rich $M_{23}C_6$ carbide as illustrated in the example of Fig. 2.

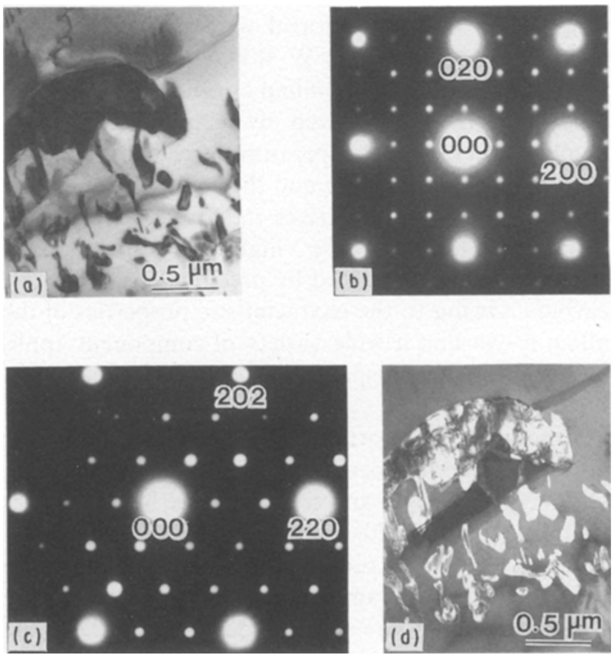

Figure 2 Identification of $M_{23}C_6$ carbide at grain boundaries in the annealed condition (specimen annealed at 1230 °C and then air-cooled). (a) Bright-field TEM image illustrating carbide precipitates. (b) Corresponding diffraction pattern in [0 0 1] orientation. (c) Corresponding diffraction pattern in [1 1 1] orientation. (d) Dark-field image formed with a carbide reflection at 1/3 position of the matrix reflection.

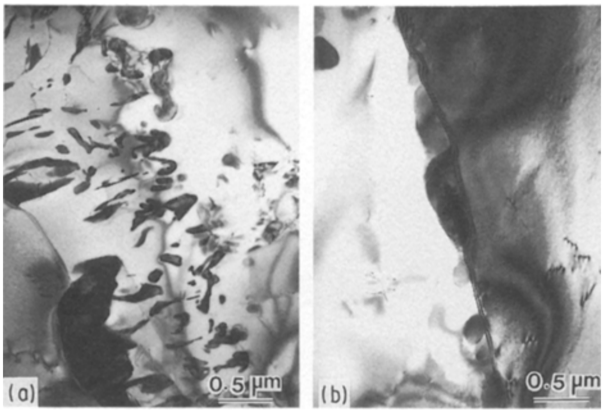

Figure 3 Bright-field TEM images illustrating the effect of cooling rate from the solution-annealing temperature (1230 °C) on the morphology of $M_{23}C_6$ carbide at grain boundaries. (a) Air-cooled, (b) water-quenched.

Characteristic reflections of the $M_{23}C_6$ carbide were observed at every one-third and all equivalent positions of the matrix reflections which typified a cube-to-cube orientation relationship [9, 10]. However, both the density and morphology of the carbide were found to be dependent upon cooling rate, as demonstrated below.

For air-cooled specimens, many of the grain boundaries contained $M_{23}C_6$ carbide which assumed a lamellar morphology typical of a discontinuous reaction as shown in Fig. 3a. In contrast, the grain boundaries of as-quenched specimens were either free of carbide or contained globular particles, as illustrated in Fig. 3b. Such a difference in carbide precipitation characteristics was found to have a significant effect on creep strength as illustrated in the next section.

Examination of the deformation substructure indicated a relatively low stacking fault energy. For example, Fig. 4 illustrates a typical deformation substructure after 20% cold reduction at room temperature. Planar arrays of dislocations were frequently observed as shown in Fig. 4, suggesting a relatively low stacking fault energy. It was demonstrated in an earlier investigation that tungsten is very effective in lowering the stacking fault energy of nickel [11]. A low stacking fault energy would be expected to increase the activation energy required for thermally activated cross-slip of screw dislocations during creep deformation.

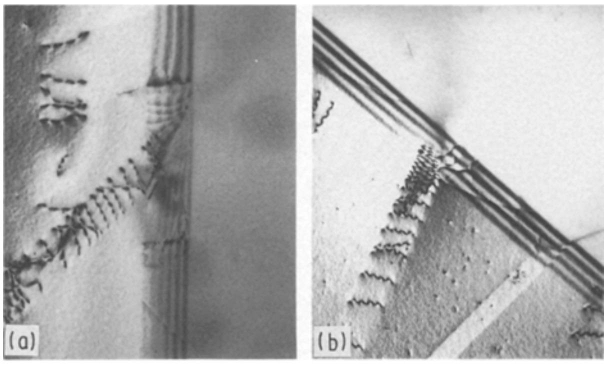

Figure 4 Bright-field TEM images illustrating planar arrays of dislocations observed in the substructure after 20% cold reduction at room temperature.

3.2. Effect of initial microstructure on creep strength

Fig. 5 illustrates typical creep curves derived from air-cooled and water-quenched specimens at 925 °C/ 40 MPa. For the air-cooled specimen which initially contained lamellar $M_{23}C_6$ carbide at grain boundaries, no steady-state creep stage could be distinguished and the creep rate was accelerated from the beginning of the test. In this case, fracture occurred with very limited ductility (~ 7% elongation). However, for the water-quenched specimen which initially contained discrete particles of $M_{23}C_6$ carbide at grain boundaries, a steady-state creep stage was well defined and the creep strain at fracture was about 33%.

For the air-cooled specimens which initially contained discontinuous precipitates of $M_{23}C_6$ carbide, grain-boundary cracks were observed at the surface during the early stages of creep deformation as illustrated in Fig. 6a. A corresponding fracture surface is shown in Fig. 6b. Oxide particles enriched in chromium and likely to be Cr_2O_3 could be distinguished at grain boundaries, suggesting intergranular oxidation. Earlier investigations indicated that grain-boundary cracks are rapidly initiated by discontinuous precipitation of $M_{23}C_6$ carbide which causes premature creep failure [12–14].

Because creep behaviour during the primary stage is quite history dependent, it could be concluded from the above observations that the initial presence of a lamellar structure of $M_{23}C_6$ carbide at grain boundaries precluded strain hardening of the material during primary creep, which resulted in an accelerated creep rate. Intergranular oxidation as observed in Fig. 6 could be correlated with the effect of discontinuous carbide precipitation on the local chromium concentration as described below.

3.3. Discontinuous precipitation of $M_{23}C_6$ carbide

Generally, all discontinuous grain-boundary reactions of importance could be classified into three main types [12, 15]. Examination of the reaction which occurred in alloy 230 was found to be of type 1 [12–15]. In this case, a supersaturated solid solution behind a migrating grain boundary is decomposed into alternate lamellae of $M_{23}C_6$ carbide and a solute-depleted solid solution.

Fig. 7 illustrates the evolution of the lamellar grain-boundary structure of $M_{23}C_6$ carbide as a function of exposure time at 925 °C. Initially, the specimens were water-quenched from the solution-annealing temperature. Noting that $M_{23}C_6$ carbide is partially coherent with the matrix, during the early stages of exposure (Fig. 7a), the carbide assumed a platelet-type morphology, suggesting that coherency was maintained inside one grain as proposed in the pucker mechanism

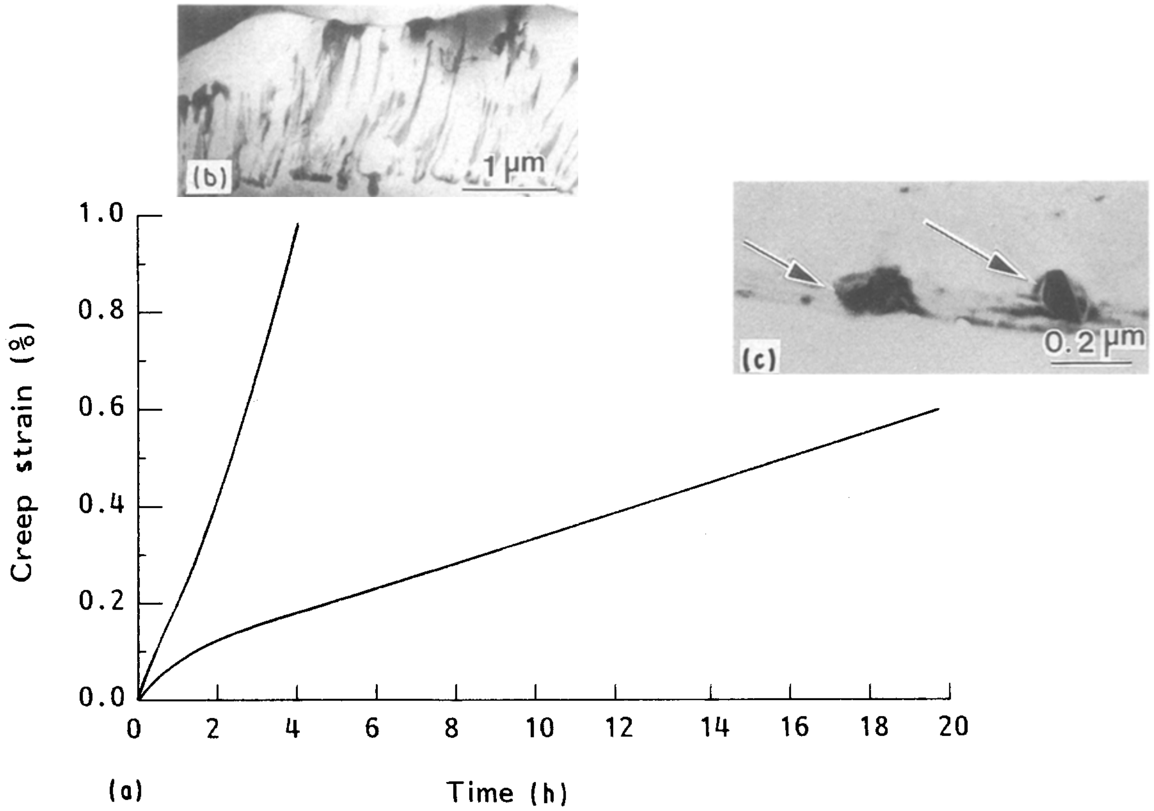

Figure 5 (a) Effect of cooling rate from the solution-annealing temperature (1230 °C) on creep curves derived at 925 °C/40 MPa. Initial carbide morphologies are shown in the bright-field STEM images of the insets; (b) air-cooled, (c) water-quenched.

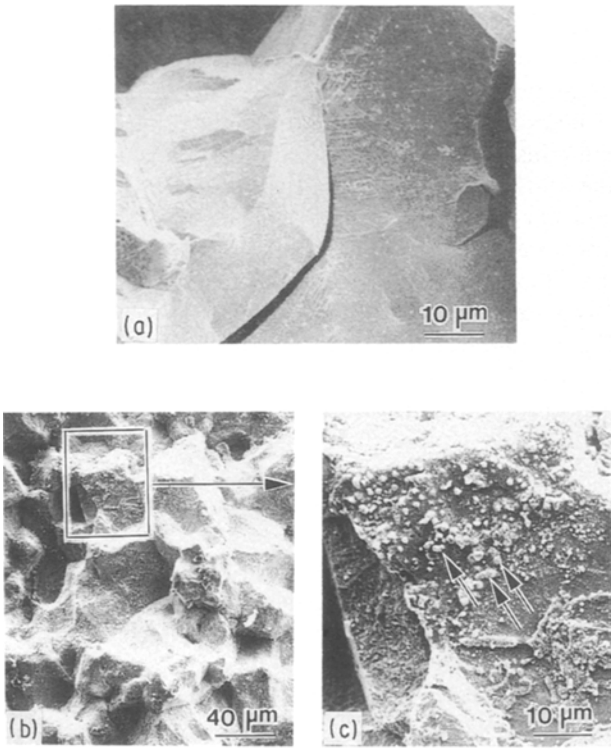

Figure 6 Secondary electron SEM images illustrating creep fracture characteristics (925 °C/40 MPa) of an air-cooled specimen. (a) Intergranular surface crack (~ 0.4% creep strain). (b) Fracture surface (same area observed at different magnifications, oxide particles are indicated by the arrows).

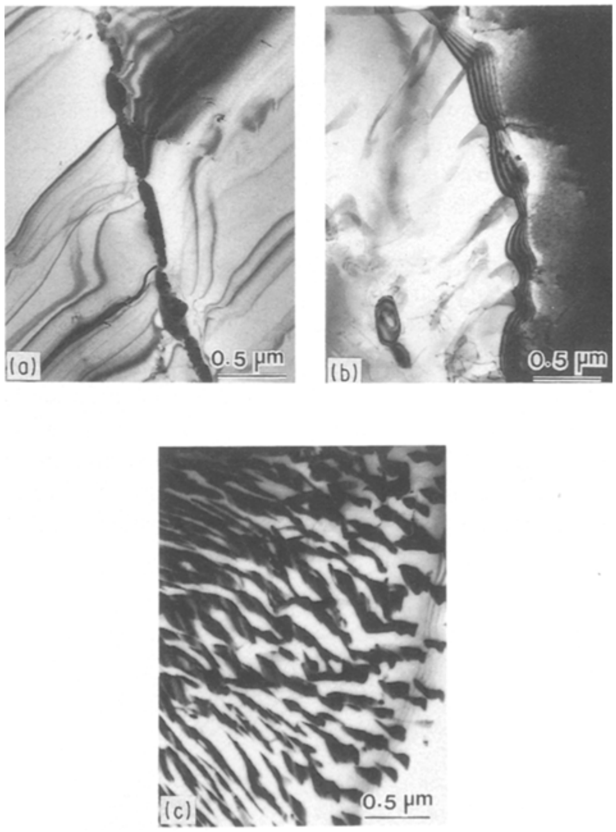

Figure 7 Bright-field TEM images illustrating the evolution of the lamellar grain-boundary structure of $M_{23}C_6$ carbide during exposure at 925 °C, for (a) 5 min, (b) 15 min, (c) 1 h.

[16, 17]. With continued exposure, the grain boundary migrated along the direction of higher interfacial energy, leaving behind carbide precipitates inside the grain where the interfacial energy was lower (Fig. 7b). Further migration of the grain boundary increased the carbide density and resulted in a lamellar structure such as that shown in Fig. 7C.

Generally, during exposure at 925 °C in the absence of an external stress, the extent of grain-boundary precipitation of $M_{23}C_6$ carbide was considerably more pronounced in comparison with intragranular precipitation. However, as shown later, intragranular precipitation was promoted in the presence of an external stress.

Fig. 8 illustrates the result of microchemical analysis of the grain-boundary carbide using an ultra-thin window X-ray detector. As expected of a type 1 discontinuous reaction, the matrix solid solution in between the $M_{23}C_6$ carbide was found to be chromium-depleted. A concentration profile of chromium across the lamellar structure as produced by point analysis is shown in Fig. 9. Owing to localized depletion in chromium the oxidation resistance alongside grain boundaries would be considerably reduced. Provided a grain-boundary crack was initiated at the surface (Fig. 6a), intergranular oxidation would be promoted, which is consistent with the observation of Fig. 6b. Commonly, this is referred to as stress-assisted intergranular oxidation. Such behaviour could contribute to premature creep failure.

Even when the material was rapidly cooled to suppress the discontinuous precipitation reaction, it would be expected to occur during elevated temperature creep as demonstrated in Fig. 7. However, the behaviour illustrated in Fig. 7 appeared to be modified by the presence of an external stress, as described below.

3.4. Strain hardening during primary creep

Examinations of crept specimens (initially water-quenched) from interrupted tests during the primary creep stage at 925 °C/40 MPa revealed a relatively high density of intragranular $M_{23}C_6$ carbide precipitates. Preferred precipitation sites included dislocations and incoherent sides of twin boundaries as illustrated in Fig. 10.

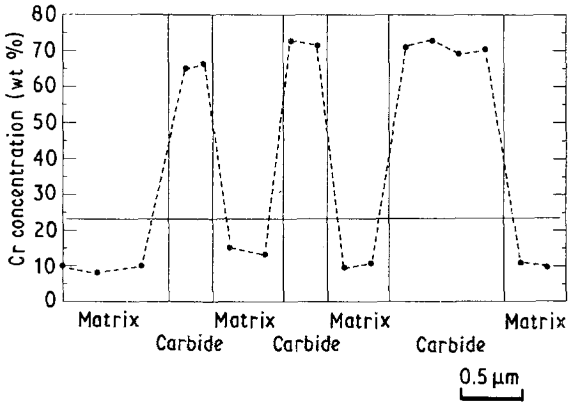

Figure 9 Concentration profile of chromium across the lamellar grain-boundary structure (specimen exposed 1 h at 925 °C) as produced by point analysis. (———) Bulk chromium concentration.

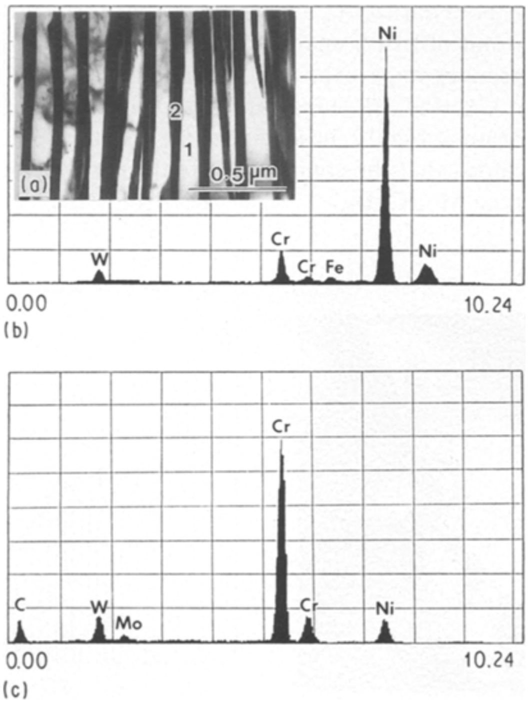

Figure 8 Microchemical analysis of the lamellar grain-boundary structure developed after 1 h exposure at 925 °C. (b) X-ray spectrum derived from the matrix region 1 in (a). (c) X-ray spectrum derived from the carbide region 2 in (a).

A dislocation configuration such as that shown in Fig. 10a was maintained after up to 60° tilt angle of thin-foil specimens suggesting that the dislocations were not lying in the plane above or below that of the carbide particles. Instead, it appeared that there was an attractive interaction between the dislocations and the carbide particles. Such a type of dislocation–particle interaction is known as "departure-side pinning" and was found to be operative in oxide dispersion-strengthened alloys [18–21]. In this case, the dislocations remain in intimate contact with the particles. Based upon the spectral data of Fig. 10b, it could be concluded that the composition of the carbide was of the type $Cr_{21}(W, Mo)_2C_6$. As illustrated in Fig. 10c, the carbide precipitated at the incoherent side of the twin boundary (encircled regions) and then grew parallel to the coherent sides, i.e. parallel to $\{1\,1\,1\}$ planes.

In contrast to the above case, a considerably smaller density of $M_{23}C_6$ carbide was observed in the matrix of specimens exposed for the same period of time at 925 °C in the absence of an external stress. It is to be noted that precipitation of $M_{23}C_6$ carbide in austenitic stainless steels was found to be strongly influenced by a stress field [22]. Although the exact mechanism remains to be established, it is apparent from the above results that the comparatively higher defect density in as-quenched specimens, e.g. vacancies, promoted intragranular precipitation of $M_{23}C_6$ carbide in the presence of an external stress.

As expected, the alloy exhibited a work-hardened substructure during primary creep. Fig. 11 summarizes typical dislocation substructures observed during the primary creep stage. Slip lines could be clearly distinguished in Fig. 11a with evidence of cross-slip. Frequently, immobile dislocation pairs were observed in the substructure as illustrated in Fig. 11b and c. Such pairs could form when a moving dislocation develops an irregular shape by encountering non-uniformly distributed solute atoms. Close pairs, such

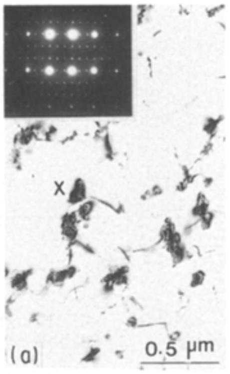

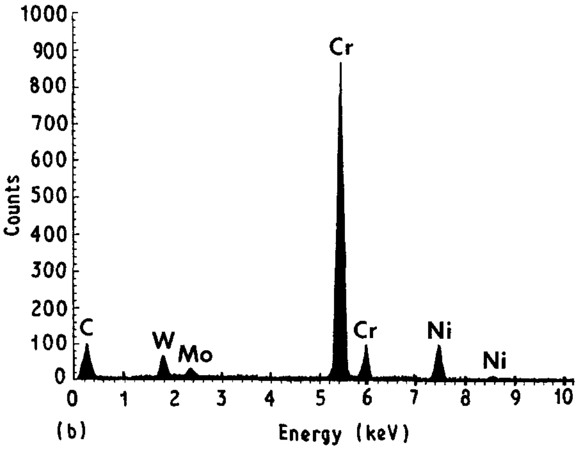

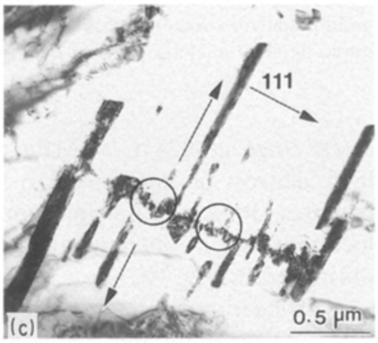

Figure 10 Intragranular precipitation of $M_{23}C_6$ carbide during primary creep of a water-quenched specimen (925°C/40 MPa). (a) Bright-field TEM image illustrating $M_{23}C_6$ carbide precipitates at dislocations: a $\langle 1\ 1\ 2\rangle$ microdiffraction pattern derived from the particle marked ($\times$) is shown in the inset. (b) X-ray spectrum derived from the particle marked ($\times$) in (a). (c) Bright-field TEM image illustrating $M_{23}C_6$ carbide precipitates at a twin boundary.

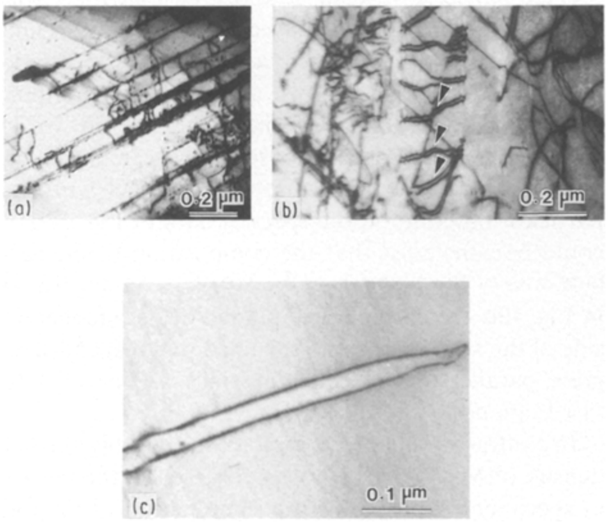

Figure 11 Bright-field TEM images illustrating typical dislocation substructures observed during primary creep of a water-quenched specimen (925 °C/40 MPa). (a) Slip lines with evidence of cross-slip. (b) Dislocation-pairs indicated by the arrows. (c) A high-magnification image of an immobile close pair.

as that shown in Fig. 11c, would be expected to contribute to strain hardening because they increase the length of immobile dislocations.

In agreement with the result of Fig. 5, it could be concluded that initial suppression of the discontinuous reaction by rapid cooling promoted strain hardening during primary creep. For a type 1 discontinuous grain-boundary reaction, as in the present case, heterogeneous nucleation of precipitates in the matrix promoted by a sufficiently high defect density (Fig. 10a) was reported to suppress discontinuous grain-boundary precipitation [23]. Another effect of rapid cooling appeared to be a more effective utilization of boron as described below.

3.5. Role of boron

Boron is known to segregate to various planar defects such as stacking faults, antiphase boundaries, twin boundaries as well as to dislocations [24]. Microchemical analysis by electron energy loss spectroscopy (EELS) of crept specimens from interrupted tests during primary and steady-state creep revealed a considerable segregation of boron to $M_{23}C_6$ carbide at grain boundaries. As an example, Fig. 12 illustrates the result of EELS analysis for a specimen crept into the primary stage (exposed 15 min at 925 °C/40 MPa). Both C*K* and B*K* edges are observed in the EELS spectrum of Fig. 12. Based upon this result, it could be concluded that the composition of the carbide was of the type $M_{23}(C, B)_6$.

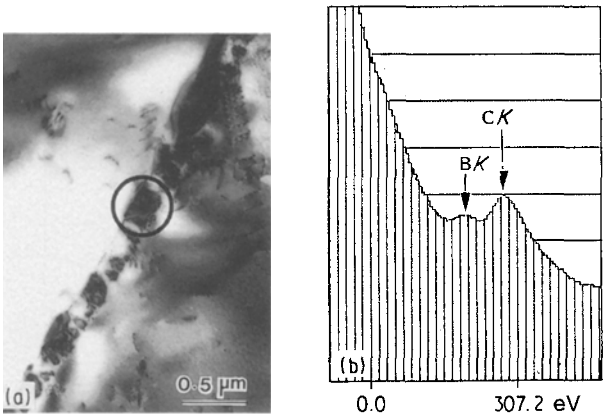

Figure 12 An example illustrating boron segregation to $M_{23}C_6$ carbide precipitates at a grain boundary. (a) Bright-field TEM image. (b) Electron energy loss spectrum derived from the encircled carbide precipitate in (a).

Comparison of Fig. 12a with Fig. 7b (specimen exposed 15 min at 925 °C in the absence of an external stress) revealed that in the presence of an external stress, the lamellar carbide morphology was replaced by a globular morphology, suggesting that the discontinuous reaction was suppressed. Although, the composition of the carbide in Fig. 7b was also found to be of the type $M_{23}(C, B)_6$, the beneficial effect of boron on creep strength would be expected to become more pronounced in the presence of the globular morphology (Fig. 12a). It was suggested that as a result of boron segregation to the carbide, it becomes more effective in resisting the formation of grain-boundary wedge cracks and cavities because of increase in its lattice constant, stability and/or cleavage strength [25].

Suppression of the discontinuous reaction was also reflected by the microstructural changes during steady-state creep as described below.

3.6. Steady-state microstructure

Generally, the extent of discontinuous precipitation in crept specimens was found to be less pronounced in comparison with uncrept specimens after the same exposure conditions.

For crept specimens, the $M_{23}C_6$ carbide continued to precipitate at matrix dislocations. Simultaneously a subgrain structure was well developed as illustrated in Fig. 13.

As pointed out earlier, there was evidence for attractive interaction between dislocations and carbide particles precipitated during primary creep (Fig. 10a). Owing to this interaction, the substructure contained tangles of dislocations prior to the onset of steady-state creep. This suggested that the creep rate was controlled at least partially by mobile dislocations cutting through the tangle. However, experimental observations indicated that more than one strain-producing mechanism were operative, as demonstrated below.

Typical dislocation arrangements at the subboundaries and in the interiors of the subgrains are summarized in Fig. 14. Generally, the subboundaries were not lying parallel to crystallographic planes, as can be seen from Fig. 14a and b. Dislocations bowing out at the subboundaries were observed, as indicated by the arrows in Fig. 14a. This appeared to be consistent with the unlikely event that a moving dislocation can cut through a subboundary into the neighbouring subgrain. As illustrated in Fig. 14c, slip lines were observed in the interiors of the subgrains with evidence of cross-slip. Growth of a slip band could then be dependent upon dislocations bowing out at subboundaries. Also, the interiors of the subgrains contained jogged screw dislocations as shown in Fig. 14d. Possibly, these jogs were acquired when mobile dislocations passed through a tangle such as that shown in Fig. 13. Motion of these jogged dislocations would be dependent upon generation of vacancies. It is well

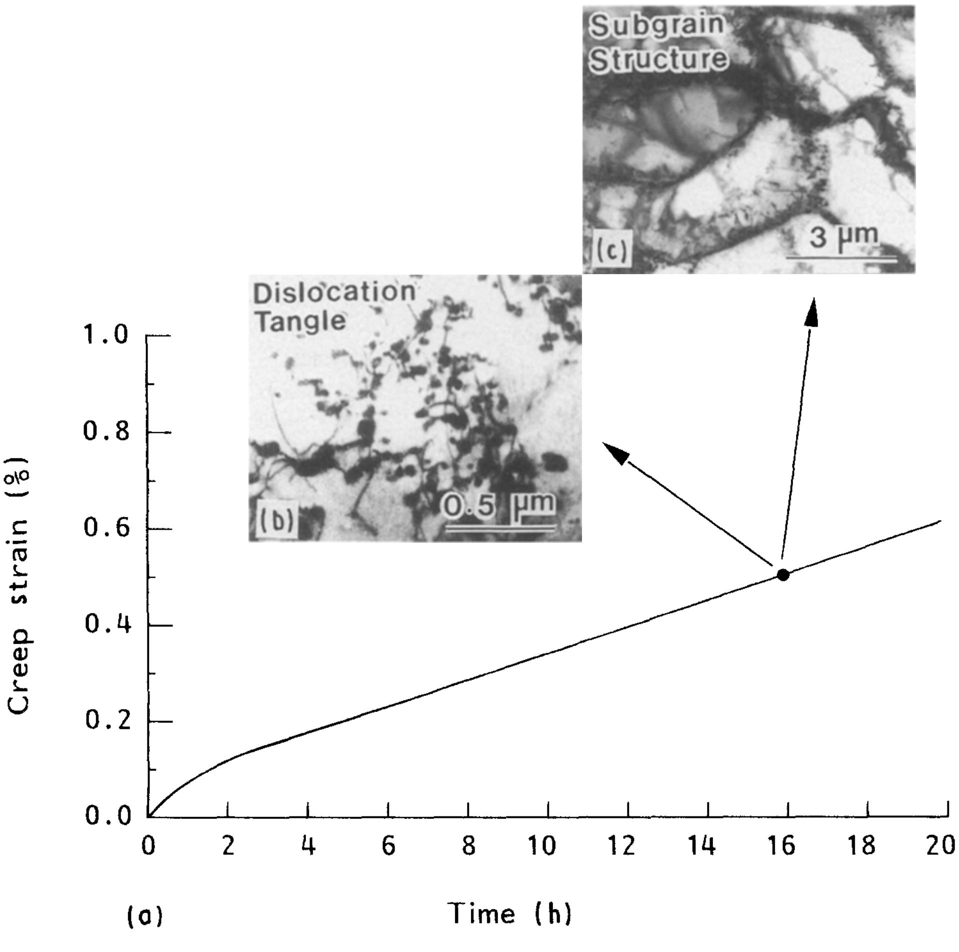

Figure 13 (a) A creep curve derived from a water-quenched specimen at 925 °C/40 MPa and (b, c) bright-field TEM images illustrating typical dislocation substructures after ~ 0.5% creep strain.

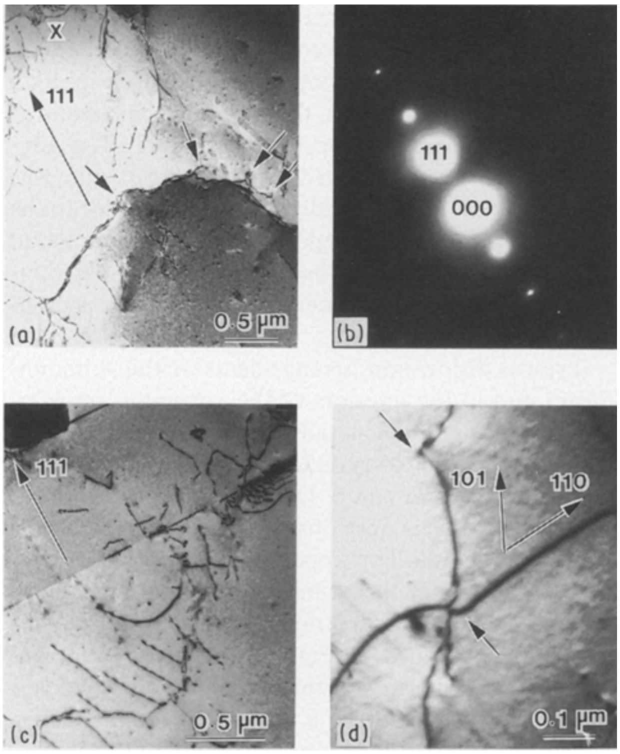

Figure 14 Distribution of dislocations in the subgrain structure formed during steady-state creep of a water-quenched specimen at 925 °C/40 MPa (~ 0.5% creep strain). (a) Bright-field TEM image illustrating dislocations bowing out at a subboundary as indicated by the arrows. (b) Corresponding diffraction pattern. (c) Bright-field TEM image illustrating slip lines with evidence of cross-slip in the region adjacent to (×) in (a). (d) Bright-field TEM image illustrating jogged screw dislocations in the interior of a subgrain (jogs are indicated by the arrows).

known that grain boundaries act as sources of vacancies [26]. However, in comparison with a high-angle boundary, a low-angle boundary is considerably less effective as a source of vacancies. Consequently, the mobility of dislocations such as those shown in Fig. 14d would be rather restricted.

Another important observation was the generation of dislocations at segments of high-angle grain boundaries not occupied by carbide precipitates. Fig. 15 illustrates dislocations bowing out at a high-angle grain boundary. This observation suggested that the creep rate was influenced by grain size. However, this behaviour remains to be established.

Based upon the above results, it appeared that there was more than one creep mechanism simultaneously operative such as: (1) bowing out of dislocations at subboundaries, (2) cross-slip, (3) motion of jogged screw dislocations, and (4) generation of dislocations at high-angle grain boundaries.

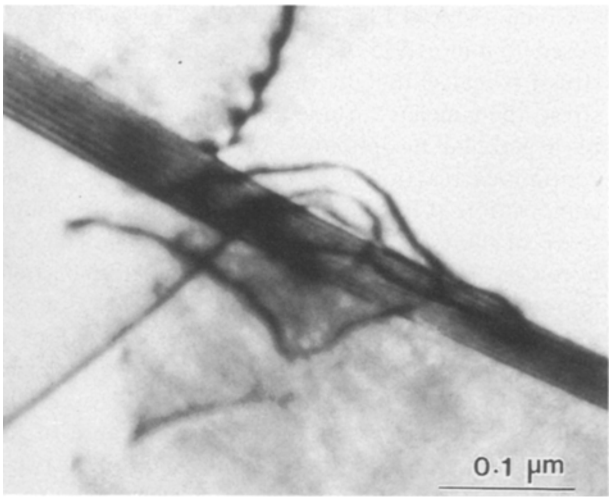

Figure 15 Bright-field TEM image illustrating a dislocation source at a high-angle grain boundary during steady-state creep of a water-quenched specimen (925 °C/40 MPa).

4. Conclusion

Based upon the results of this investigation, it could be concluded that the creep strength of alloy 230 is promoted by (1) pinning of grain boundaries by tungsten-rich M_6C carbide, (2) relatively low stacking fault energy, and (3) boron segregation to grain-boundary $M_{23}C_6$ carbide. However, the beneficial effects of these parameters were suppressed by the initial presence of discontinuously precipitated $M_{23}C_6$ carbide at grain boundaries. By means of a proper heat treatment, the discontinuous reaction was suppressed and intragranular precipitation of the carbide was promoted, presumably due to sufficiently high defect density in the matrix. Intragranular carbide precipitates were found to interact attractively with dislocations. During steady-state creep, a number strain-producing mechanisms, including (1) bowing out of dislocations at subboundaries, (2) cross-slip, (3) motion of jogged screw dislocations, and (4) generation of dislocations at high-angle boundaries, appeared to be operative simultaneously.

Acknowledgements

The support of the Research Institute, King Fahd University of Petroleum and Minerals, and permission to publish this work, are greatly appreciated.

References

1. H. M. TAWANCY, D. L. KLARSTROM and M. F. ROTHMAN, *J. Metals.* **36**(9) (1984) 58.
2. D. L. KLARSTROM, H. M. TAWANCY, D. E. FLUCK and M. F. ROTHMAN, in "29th International Gas Turbine Conference", ASME Paper no. 84-GT-70 (ASME, New York, 1984).
3. Y. MONMA, in "Superalloys, Supercomposites and Superceramics", edited by J. K. Tien and T. Caulfield (Academic Press, New York, 1989) p. 339.
4. J. BRESSERS (ed.), "Creep and Fatigue of High Temperature Alloys" (Applied Science, London, 1981) p. 145.
5. L. BENDERSKY, A. ROZEN and A. K. MUKHERJEE, *Int. Met. Rev.* **30**(1) (1985) 1.
6. BRIAN RALPH, in "Grain-Boundary Structure and Kinetics", ASM Materials Science Seminar (ASM, Metals Park, OH, 1980) p. 181.
7. J. O. NILSSON, P. R. HOWELL and G. L. DUNLOP, *Acta Metall.* **27** (1979) 179.
8. G. L. DUNLOP, J. O. NILSSON and P. R. HOWELL, *J. Microsc.* **116** (1979) 115.
9. H. M. TAWANCY, *J. Mater. Sci.* **18** (1983) 2976.
10. J. W. EDINGTON, "Typical Electron Microscope Investigations" Philips, Gloeilampenfabrieken, Eindhoven, 1976) p. 38.

11. T. C. TIEARNEY and N. J. GRANT, *Met. Trans.* **13A** (1982) 1827.
12. D. B. WILLIAMS and E. P. BUTLER, *Int. Met. Rev.* **26**(3) (1981) 153.
13. R. B. SCARLIN, *Scripta Metall.* **10** (1976) 711.
14. P. S. KOTVAL and H. HATWELL, *Trans. AIME* **245** (1969) 1821.
15. M. N. THOMPSON, PhD thesis, University of Cambridge (1971).
16. K. N. TU and D. TURNBULL, *Acta Metall.* **15** (1967) 369.
17. *Idem, ibid.* **15** (1967) 1317.
18. A. H. COOPER, V. C. NARDONE and J. K. TIEN, in "Superalloys, Supercomposites and Superceramics" edited by J. K. Tien and T. Caulfield (Academic Press, New York, 1989) p. 357.
19. J. H. SCHROER and E. ARZT, *Script Metall.* **19** (1985) 1129.
20. V. C. NARDONE, D. MATEJCZYK and J. K. TIEN, *Acta Metall.* **32** (1984) 1509.
21. V. C. NARDONE and J. K. TIEN, *Scripta Metall.* **17** (1983) 467.
22. N. TERAO and B. SASMAL, *Metallogr.* **13** (1980) 117.
23. E. HORNBOGEN, *Metal. Trans.* **3** (1972) 2717.
24. J. D. DESTAFANI, *Adv. Mater. Process.* **115**(2) (1989) 37.
25. C. HAMMOND and J. NUTTING, *Met. Sci. J.* **11** (1977) 474.
26. R. W. BALLUFFI, in "Grain-Boundary Structure and Kinetics" (ASM Materials Science Seminar, Metals Park, OH, 1980) p. 297.

Received 2 September 1991
and accepted 16 January 1992